

Application and Comparison of Deep Learning Methods in the Prediction of RNA Sequence Degradation and Stability

Ankit Singhal

February 2021

Abstract

mRNA vaccines are receiving increased interest as potential alternatives to conventional methods for the prevention of several diseases, including Covid-19. This paper proposes and evaluates three deep learning models (Long Short Term Memory networks, Gated Recurrent Unit networks, and Graph Convolutional Networks) as a method to predict the stability/reactivity and risk of degradation of sequences of RNA. These predictions can be very useful in the development of mRNA vaccines as they can reduce the number of sequences synthesized and tested by helping to identify the most promising candidates. Reasonably accurate results were able to be generated with the Graph Convolutional Network being the best predictor of reactivity (RMSE = 0.249) while the Gated Recurrent Unit Network was the best at predicting risks of degradation under various circumstances (RMSE = 0.266). Overall, combining all target variables, the GRU performed the best with an accuracy value of 76%. Results suggest feasibility of applying such methods in mRNA vaccine research in the near future.

Contents

1	Introduction	3
2	Materials and Methods	4
2.1	Materials	4
2.1.1	Software/Packages Used	4
2.1.2	Dataset Description	4
2.1.3	Data Representation	5
2.2	Methods and Models	6
2.2.1	Data Processing and Overall Model Architecture	6
2.2.2	Machine Learning, Deep Learning, and Neural Networks Background	7
2.2.3	Long Short Term Memory Networks	9
2.2.4	Gated Recurrent Unit Networks	10
2.2.5	Graph Convolutional Networks	11
2.2.6	Performance Assessment	11
3	Results	12
3.1	Initial Training and Validation	12
3.2	Model Comparison	13
4	Discussion and Conclusion	15
5	Appendix	19
5.1	Figure 12 - Hot encoding	19
5.2	Figure 13 - Basic Artificial Neural Network Architecture	20
5.3	Figure 14 - LSTM Diagram	21
5.4	Figure 15 - GRU Diagram	22
5.5	Figure 16 - GCN Diagram	23
5.6	Figure 17 - Loss Function Error Term Comparison	24

1 Introduction

Over the last two decades, there has been increasing interest in the field of RNA-based technologies in the creation of prophylactic vaccines. They are widely regarded to be plausible alternatives to conventional approaches due to their high potency, capacity for quick and low-cost manufacturing, and relatively safe administration. They are currently being researched for many diseases, with the Pfizer-BioNTech vaccine against SARS-CoV-2 being the first to be approved for human use [1–3]. One of the primary barriers in the creation of such therapeutics is the fragility of the RNA molecule; they are susceptible to rapid degradation within minutes to hours [4] and as such need to be freeze dried or incubated at low temperatures in order to be kept stable. In the current pandemic, vaccines are seen as the most promising means to control the novel coronavirus, but with current limitations on mRNA vaccines, efficient *in vivo* delivery of such mRNA molecules seems improbable; it would likely only reach a fraction of the population, mostly relegated to countries with a higher level of infrastructural development [5].

Therefore, research into the the stability and degradation of RNA molecules has received continued interest, to date largely consisting of traditional statistical approaches and biophysical models. However, it still remains unclear exactly which parts of RNA molecules are more prone to spontaneous degradation and thus difficult to accurately predict the reactivity and degradation of mRNA [6]. Therefore, experimentation, an incredibly time consuming process, is the default method in determining these values.

The aim of this manuscript is to present three possible Deep Learning approaches to this problem through the usage of the Stanford OpenVaccine dataset. Two variants of Recurrent Neural Networks (RNNs) are employed, Long Short Term Memory Networks (LSTMs) and Gated Recurrent Unit Networks (GRUs), along with a variant of a Graph Neural Network (GNN), the Graph Convolutional Network (GCN). These models are applied and compared to assess whether Machine Learning methods can provide helpful results in predicting the reactivity and degradation of mRNA molecules. This can save significant resources in the development of mRNA vaccines by helping identify the most promsing candidates using in silico methods.

2 Materials and Methods

2.1 Materials

2.1.1 Software/Packages Used

The majority of this work was done in the Python programming language using a TensorFlow back end with a surface level Keras API. Refer to Table 1 for all the software/packages used throughout the creation and testing of the models along with related information [7–15].

Software/Package	Use	Developer
Python 3.7	Used to write the code for the models discussed.	Python Software Foundation
TensorFlow	Used as a backend for the majority of the models presented.	Google
Keras	Used as a high level API for some parts of the model.	Google
SKLearn	Used for k-Fold Cross Validation.	Cornapeau and Matthieu
Pandas	Used for data handling.	McKinney
Numpy	Used for data handling.	Oliphant
Matplotlib	Used to create figures in manuscript.	Droettboom and Caswell
ARNiE	Used to generate augmentation data.	DAS Labs

Table 1: All the packages/software used in the creation of the models presented.

2.1.2 Dataset Description

The dataset used in this manuscript to evaluate the models is called the ”Stanford OpenVaccine” dataset [16]. It consists of 6034 RNA sequences. The training/validation set consisted of 3029 of these sequences with a length of 107 nucleotide bases. The testing dataset consists of 3005 sequences with a length of 130 nucleotide bases. Due to experimental limitations (in collecting the data according to the researchers at Stanford [16]), measurements on the final bases in the sequences cannot be carried out, therefore, only 68 (for the sequences with length 107) and 91 (for the sequences with length 130) of the first bases in the respective sequences have experimental data associated with them.

Three predictors were associated with each sequence: the sequence itself (described in A,G,C, and U bases), the expected structure of the molecule, and the Predicted Loop Type (derived from a simulation of the secondary structure of the RNA molecule). A Base Pair Probability Matrix was also provided for each individual sequence indicating the probability of certain base-pair interactions. Five experimentally-determined sets of values (henceforth referred to as ’target values’) were also given for the first 68 or 91 base

pairs in the sequence: Reactivity values, degradation values at pH 10, degradation values at pH 10 with added Magnesium, degradation values at 50°, and degradation values at 50° with added Magnesium. Refer to Table 2 for more information.

Feature	Classification	Description	Sample
Sequence	<i>Input</i>	A sequence of 107 letters corresponding to the four bases in the sequence. Expected structure of the molecule (length = 107). '(` and `)' refer to a base pair interaction. All ',' in the middle are associated with no BP interactions.	A, G, U, U, C, ... (..()...)(... ...)
Structure	<i>Input</i>	Predicted secondary structure of the RNA molecule at different points. 'S' refers to a stem structure, 'M' multiloop, 'I' internal loop, 'B' bulge, 'H' hairpin loop, 'E' dangling end, 'X' external loop.	S, S, M, S, H, ...
Predicted loop type	<i>Input</i>	Reactivity values at each individual point in the sequence.	1.23, 3.46, ...
Reactivity	<i>Target</i>	Degradation values at pH 10.	0.89, 2.44, ...
Deg pH 10	<i>Target</i>	Degradation values at pH 10 with added Mg.	1.28, 0.88, ...
Deg pH 10 Mg	<i>Target</i>	Degradation values at 50°C.	2.02, 1.87, ...
Deg 50°C	<i>Target</i>	Degradation values at 50°C with added Mg.	1.11, 2.44, ...
Deg 50°C Mg	<i>Target</i>		

Table 2: Inputs and target features of the Stanford OpenVaccine dataset.

The task of the algorithms that are presented in this paper is to take the sequence and other structural features of an RNA molecule (features marked as 'inputs') and predict its stability (through the five target values).

2.1.3 Data Representation

As mentioned earlier, each base of the sequence has five target and two further structural features associated with it. This will be represented as a feature matrix for all three ML models. What is of particular interest however, is the Base Pair Probability Matrix associated with each sequence which takes the form $N \times N$, where N is the number of bases in the sequence. It can be represented as a standard matrix (refer to Figure 1 for visualization) or as a graph (refer to Figure 2) with nodes and edges. This distinction is important for the former form is used for the two RNN architectures whereas the latter is used for the GCN.

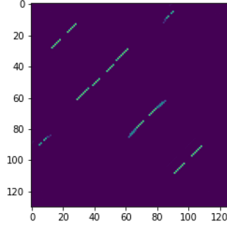


Figure 1: Visualization of a sample BPPM Matrix. Purple indicates no base pair interaction, the more green a color, the higher the interaction between those two bases (produced by author).

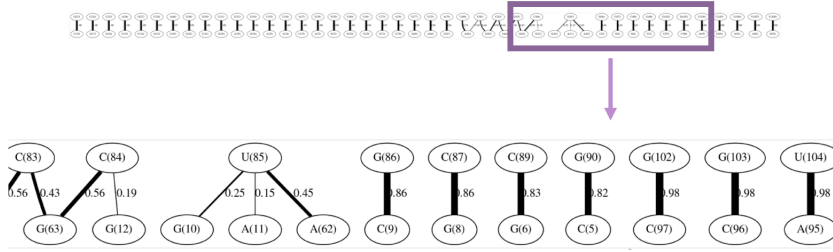


Figure 2: Visualization of a sample graph structure of a BPPM. Information in the nodes correspond to the type of base and its place on the sequence, the width and number next to the edges refer to the interaction between the two bases with values ranging from 0-1 (produced by author).

2.2 Methods and Models

2.2.1 Data Processing and Overall Model Architecture

Data from the dataset was first mapped to vector matrices and hot encoded, to ensure the data could be processed by a computer. Essentially, they were mapped onto a vector of the shape $1 \times n$ where n is the number of possible options present for that specific feature. For example, since there are four nitrogenous bases, the vector shape to denote a single base was 1×4 and the total sequence vector for one strand of RNA took the shape $1 \times 4 \times 107$ (refer to Table 2 and Figure 12 for information about the number of features and a visual explanation of the hot encoding process, respectively).

After splitting the training and testing data according to the specifications lined out in Section 2.1.2, the training data was augmented using the ARNiE package, the same package used to create the data in the first place. Data augmentation is a technique to artificially create new training data from the existing data to improve the performance of ML models [17]. The

part of the package, Vienna2, that was originally used to predict the RNA structures for the sequences, is based off of thermodynamic experiments and finds the structure by modelling the position of the lowest possible entropy. To augment the data, an alternate method was employed, CONTRAfold, that uses statistical methods to predict the structure. Therefore, for every sequence, new structures and predicted loop types were generated, effectively allowing for the training data to be doubled.

Finally, the resulting data was used to create the model using the architectures explained in Figure 3 and the model was evaluated on the testing data. In terms of hyperparameter optimization, the number of epochs was set to 50 and the batch size was set to 64. K-Fold cross validation was also conducted with $k = 4$. These values were determined through a simple grid search method to find the optimal quantity/quantity after which returns were negligible. An ADAM optimizer was also utilized with the learning rate set to a standard $1.0 \cdot 10^{-3}$, due to the fact that the model was running on a Tensorflow backend.

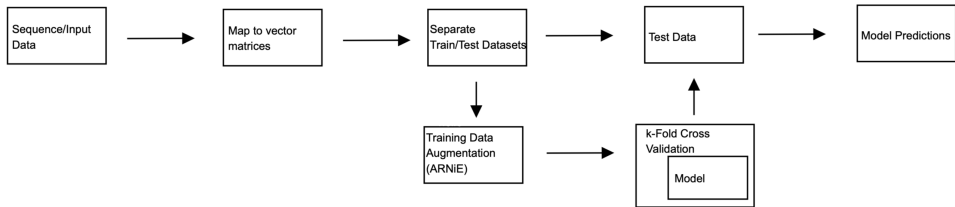


Figure 3: High level diagram of the overall model architecture. 'Model' in the diagram refers to one of the three ML approaches discussed in the next section (produced by author).

2.2.2 Machine Learning, Deep Learning, and Neural Networks Background

Although words such as 'Artificial Intelligence', 'Machine Learning', 'Deep Learning', and 'Neural Networks' have become popularized as buzzwords and seem to be synonymous with one another, there are important distinctions between them that must be understood.

Artificial Intelligence is the broadest term that denotes any computational technique that allows an algorithm to mimic human behaviour by making decisions based on logic. It was first coined by John McCarthy in 1956 [18] and over the past 60 years fields within AI have undergone rapid advancement including but not limited to: searching algorithms, evolutionary computation,

and robotics[19–21].

Machine Learning is one such subfield in AI that refers to the techniques that give computers the ability to learn and carry out tasks without explicitly programmed instructions. This usually entails a program performing statistical operations on a large dataset and discovering underlying patterns. For example, a Support Vector Machine (a type of ML algorithm) might be able to analyze labeled patient data then categorize unlabeled data into risk classes of a certain disease.

Finally, Deep Learning is an even more specific term that refers to the subset of ML which employs multi-layer neural network algorithms to learn [22]. For certain tasks, such as in Computer Vision or Natural Language Processing, the usage of such networks can recognize patterns that may be hidden to simpler forms of ML, therefore improving the performance of these algorithms.

Neural networks are computational models that are loosely based on the human brain. Neurons in the brain are connected to many other and are continuously receiving electrical impulses at their dendrites which eventually reach the cell body. Here, they are integrated in some way and, crudely speaking, once some threshold is reached, the neuron 'fires' and an impulse is transmitted to other neurons through a synapse. Nodes (or neurons) in an artificial neural network operate in a similar fashion. They receive data from a node in a previous layer, perform a learnable computation on them, then output the result to the next layer in the network (refer to Figure 13 in the Appendix for a visualization of a sample network). A general computation taking place in a single node follows the form:

$$n_{l+1} = \sigma(W_l \cdot n_l + b_l) \quad (1)$$

Where n_{l+1} is the node which is being updated, n_l represents all the previous nodes connected to n_{l+1} , W_l are the weights, b_l are the biases, and σ is the activation function. These weights and biases are learnable, i.e. these are the values that through backpropagation and gradient descent, the computer is trying to optimize. The activation function is analogous to the binary threshold of the neuron in the brain to determine whether or not it will fire, however, in modern networks, more sophisticated functions are used such as the sigmoid, ReLu, or hyperbolic tangent functions [22–24]. Figure 4 shows a visual comparison of biological and artificial neural networks.

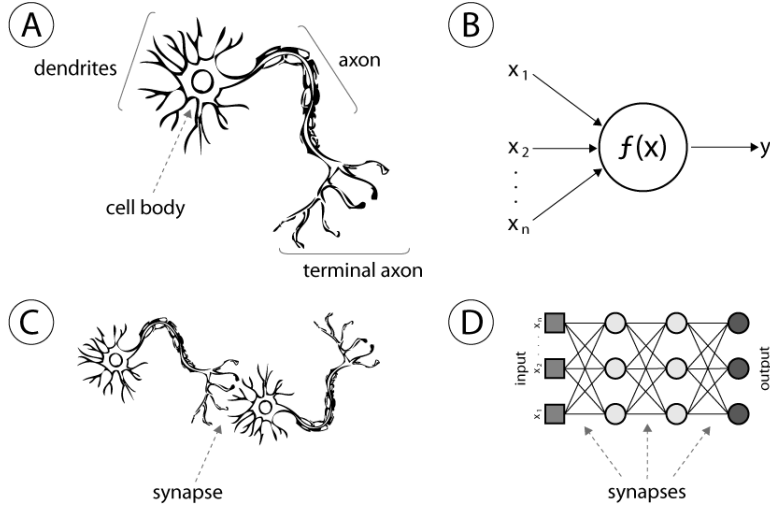


Figure 4: Comparison of neurons, nodes, synapses, and network connections between cell bodies and an artificial network (Kim [25]).

The type of neural networks that will be discussed in this paper are known as Recurrent Neural Networks (RNNs). They are, roughly speaking, repeating ANNs that allow for information through data in which spatial or temporal information is important [26]. For example, an algorithm in a messaging app that has the aim of predicting the next word in the sentence not only needs information about the preceding words in the sentence, but also the order in which they are located.

2.2.3 Long Short Term Memory Networks

A Long Short Term Memory Network (LSTM) is a type of RNN introduced by Hochreiter & Schmidhuber in 1997 [27] and further popularized by many other pieces of work following it. Like other RNNs, it essentially consists of copies of the same network in which the output of the previous network (or cell) informs the next one, allowing information to persist. A single cell in an LSTM, consists of four distinct neural network layers, three of which are ones that make 'decisions' about the persistence of information as shown in equations 2 - 4:

$$f_t = \sigma(W_f[h_{t-1}, x_t] + b_f) \quad (2)$$

$$i_t = \sigma(W_i[h_{t-1}, x_t] + b_i) \quad (3)$$

$$o_t = \sigma(W_o[h_{t-1}, x_t] + b_o) \quad (4)$$

Here the output of the previous cell along with the new input is passed through a basic neural layer with a non-linear activation function (traditionally sigmoid functions were used but in this paper, all activation functions denoted by σ were ReLu). In parallel, candidate values for the cell state are also produced as shown by equation 5:

$$\tilde{C}_t = \phi_h(W_C[h_{t-1}, x_t] + b_C) \quad (5)$$

Where the activation function in this case is a hyperbolic tangent function (compressing the values between -1 and 1). Finally using these output matrices, one can then update the cell state as given by equation 6 and produce new outputs as shown in equation 7:

$$C_t = f_t \cdot C_{t-1} + \tilde{C}_t \cdot i_t \quad (6)$$

$$h_t = o_t \cdot \phi_h(C_t) \quad (7)$$

This output is then fed into the next cell (refer to diagram in Figure 14 in the Appendix). This model was used with the normal vector matrix BPPM as represented in Figure 1.

2.2.4 Gated Recurrent Unit Networks

Introduce by Cho et al. in 2014 [28], a Gated Recurrent Unit Network is a variation of traditional LSTM networks that have the primary advantage of faster computation (due to less neural nets in each cell). Like in the LSTM, decision matrices are produced through two non-linear activation function based neural networks as shown in equations 8 and 9:

$$r_t = \sigma(W_r[h_{t-1}, x_t] + b_r) \quad (8)$$

$$z_t = \sigma(W_z[h_{t-1}, x_t] + b_z) \quad (9)$$

Candidate values are also generated through a hyperbolic-tangent-based network, however, in this case it is done directly for the output as there is no cell state, unlike in an LSTM. The candidates are then chosen by the 'decision' matrices to produce the output as shown in equations 10 and 11:

$$\tilde{h}_t = \phi_h(W_h[h_{t-1}, x_t] + b_h) \quad (10)$$

$$h_t = (1 - z_t) \cdot h_{t-1} + \tilde{h}_t \cdot z_t \quad (11)$$

Like any other form of RNN, this output is then passed to the next hidden layer (refer to diagram in Figure 15 in the Appendix).

2.2.5 Graph Convolutional Networks

Graph Convolutional Networks were introduced by Kipf & Welling in 2017 [29] and provide a novel way to analyze arbitrarily structured data in the form of a graph. A GCN is not a form of an RNN although they are both connectionist models. A GCN operates on a graph defined by $G = (V, E)$ where V is the set of nodes and E the set of edges. Nodes in the graph aggregate the features of the surrounding nodes and itself and use the following neural net (refer to 12 to generate an output which is then assigned to the node:

$$h_t = \sigma(W_h \cdot D^{-1}[h_{t-1}, \hat{A}] + b_h) \quad (12)$$

Where D is the diagonal node degree matrix of the graph and \hat{A} is equal to $A + I$, A being the adjacency matrix (taking the form $N \times N$) representing the graph (in this case, the BPPM - see Figure 2). $h_0 = N \cdot F_0$ i.e. it is a feature matrix. After an output is generated, this process can be repeated each time the output of the nodes propagating outwards (refer to diagram in Figure 16 in the Appendix). Due to the localization of such a problem, I only had two repetitions, any more resulted in negligible influences.

2.2.6 Performance Assessment

The models will be evaluated based on the error produced in the prediction of the target values. The two loss measures employed in this paper are Mean Absolute Error (MAE) and Root Mean Square Error (RMSE) described in equations 13 and 14.

$$RMSE = \sqrt{\frac{\sum_{i=1}^n (\hat{y}_i - y_i)^2}{n}} \quad (13)$$

$$MAE = \frac{1}{n} \sum_{i=1}^n |\hat{y}_i - y_i| \quad (14)$$

The difference between the two metrics is that in MAE, all the errors are averaged by weighting them equally, however, since RMSE has a quadratic term, larger individual errors will be punished more than smaller ones (refer to Figure 17 in the Appendix) .

3 Results

3.1 Initial Training and Validation

After being built using the specifications discussed earlier in this manuscript, the models were trained on the 'training' dataset discussed in section 2.1.2. For k-fold cross validation, in the models presented, $k = 4$ and this was initially repeated three times to improve accuracy. The model was split into four groups for cross validation as larger values of k were found to have negligible influence on the model results. Training and validation loss (RMSE) for the three models are show in Figure 5 and Table 3.

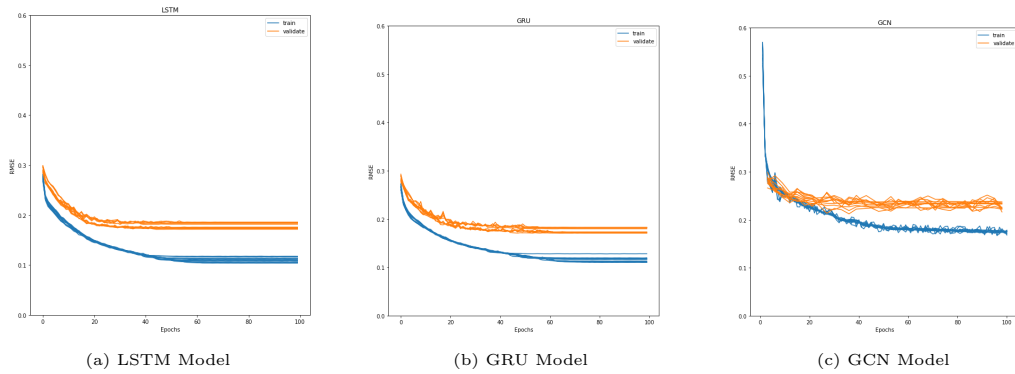


Figure 5: Training and validation loss for the twelve histories of the ML Models (produced by author).

	Training		Validation	
	RMSE	MAE	RMSE	MAE
LSTM	0.1089	0.0663	0.1758	0.1052
GRU	0.1143	0.0693	0.1787	0.1072
GCN	0.1752	0.1055	0.2232	0.1394

Table 3: Mean loss values of models after the training and validation processes.

As can be seen after the initial training and validation phase, the LSTM maintains the best performance. The GRU scores were similar to that of the LSTM, however, the GCN was in a distant third place averaging about 0.05-0.06 higher RMSE values in comparison to the other two.

3.2 Model Comparison

The performance for the three machine learning models on the training dataset are presented in Figures 6 - 10. The GRU maintained the lowest loss values for all target values, with the only exception being the reactivity (see Figure 6) and the degradation at pH 10 (only the RMSE - see Figure 7) in which the GCN had the best predictions. Notably, in Figures 8, 9, and 10, the GCN had lower RMSE values than the LSTM, however the opposite was true for the MAE values suggesting that the GCN is not as prone to large, individual errors.

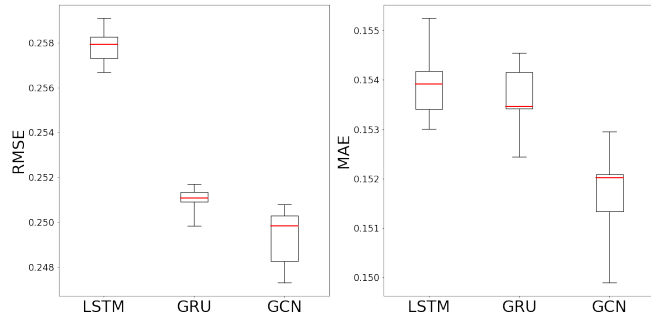


Figure 6: Results (loss) for over 20 trials of the models predicting the **reactivity** values of the training set sequences (note change in scale between plots). The GCN performed the best, both in terms of RMSE and MAE, followed by the GRU and LSTM respectively. Boxplots show the minimum, maximum, and median values along with the 25th and 75th quartiles (produced by author).

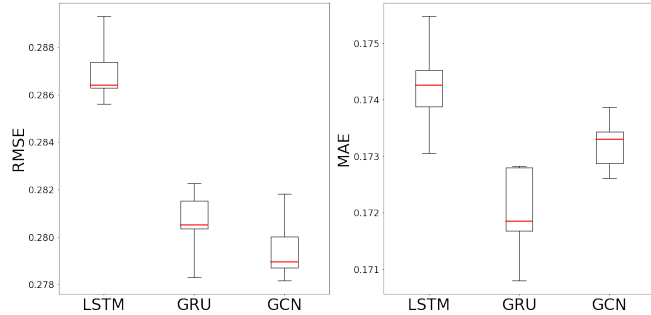


Figure 7: Results (loss) for over 20 trials of the models predicting the **degradation at pH 10** of the training set sequences (note change in scale between plots). The GCN performed the best in terms of RMSE, however, the GRU performed better in terms of MAE, suggesting the GRU is more prone to larger errors. Boxplots show the minimum, maximum, and median values along with the 25th and 75th quartiles (produced by author).

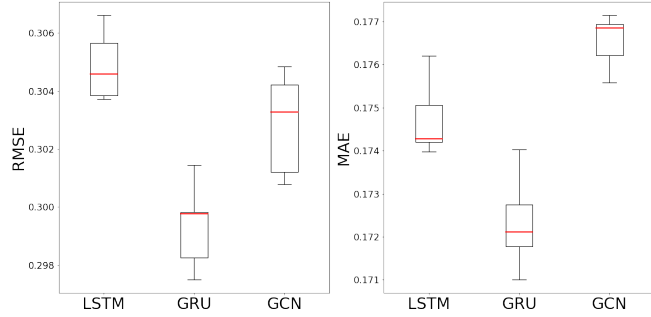


Figure 8: Results (loss) for over 20 trials of the models predicting the **degradation at pH 10 with added Magnesium** of the training set sequences (note change in scale between plots). The GRU performed the best, both in terms of RMSE and MAE, followed by the GCN in RMSE and LSTM in MAE, further reaffirming the notion that the GCN is less prone to larger individual errors. Boxplots show the minimum, maximum, and median values along with the 25th and 75th quartiles (produced by author).

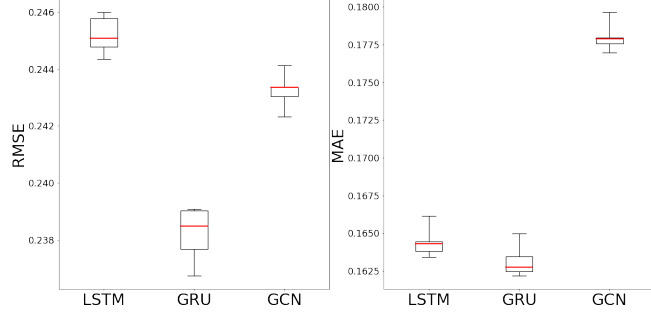


Figure 9: Results (loss) for over 20 trials of the models predicting the **degradation at 50°C** of the training set sequences (note change in scale between plots). The GRU performed the best, both in terms of RMSE and MAE, the GCN in RMSE and LSTM in MAE, similar to Figure 8. Boxplots show the minimum, maximum, and median values along with the 25th and 75th quartiles (produced by author).

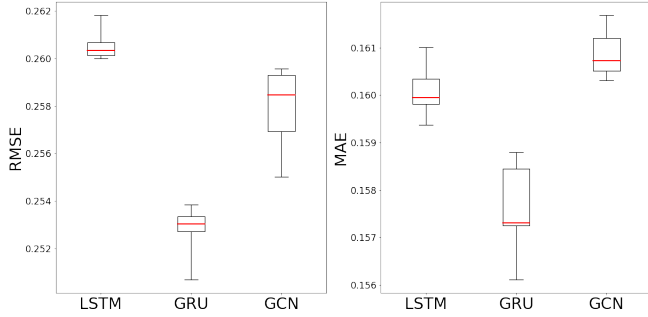


Figure 10: Results (loss) for over 20 trials of the models predicting the **degradation at 50°C with added Magnesium** of the training set sequences (note change in scale between plots). The GRU performed the best, both in terms of RMSE and MAE, the GCN in RMSE and LSTM in MAE, similar to Figures 8 and 9. Boxplots show the minimum, maximum, and median values along with the 25th and 75th quartiles (produced by author).

Mean loss across the 20 trials for each individual target were calculated along with that of all targets combined for each model. Results are shown in Figure 11.

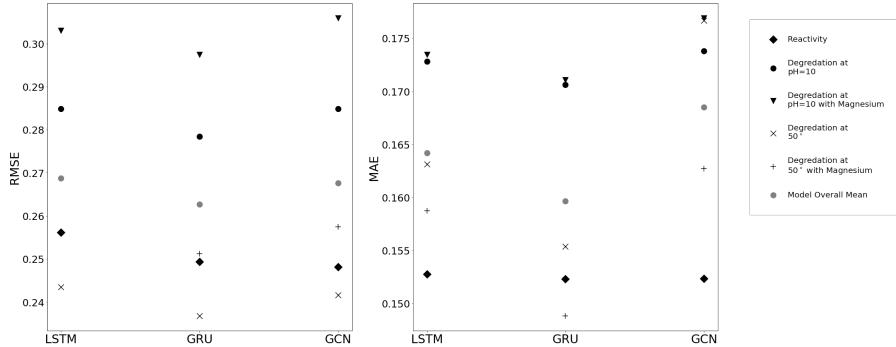


Figure 11: Mean loss results (RMSE and MAE - note change in scale between plots) for the three machine learning methods. The GRU performed the best across both metrics (produced by author).

4 Discussion and Conclusion

Although the creation of stable mRNA molecules remains difficult, datasets of sequences and corresponding information are becoming more popular and widely available. Through the use of deep learning architectures, reasonable predictions of structural features can be obtained, as demonstrated in this manuscript, with mean RMSE values ranging from 0.24 to 0.31. The usage

of such techniques has the capacity to increase the speed and efficiency of mRNA vaccine discovery and has further implications in other related fields of research.

However, such methods, as presented in this paper, are not without their limitations. It is important to note that while reasonably accurate results are produced, the error, when taking into account the scale of the values being predicted (0.5 - 4) is not insignificant; in fact, it equates to a 24% Mean Absolute Percentage Error. Therefore, this could have the potential of incorrectly predicting the stability of an important molecule which may be overlooked during the discovery phase. Thus, in its current state, as an extension, I would suggest a simple binary classification system to predict whether the molecule is stable, at the end of each of the models that would aim to minimize the False Negative rate - effectively resulting in the model being used as a screening test to remove highly unstable sequences, rather than a full-fledged research tool.

Another limitation of this method is the length of the sequences of the mRNA molecules used. The length used in this paper ranged from 107-130 bases, while an actual Covid-19 vaccine would likely range from 3000-4000 [2] bases long. As an improvement, this model could be trained on and applied to longer RNA sequences to see how this impacts the accuracy of such methods.

Despite these limitations, the results of this work show that such prediction algorithms are feasible and have the potential to save time during research processes, an especially valuable commodity during disease outbreaks. In the long term, such techniques may also better help researchers in understanding the reasoning behind the stability of certain RNA molecules and aid in the development of related technologies. It is hoped that this work will be of some use to other data scientists as well in creating better prediction models for this field.

References

- (1) Pardi, N.; Hogan, M. J.; Porter, F. W.; Weissman, D. *Nature reviews Drug discovery* **2018**, *17*, 261.
- (2) Zhang, C.; Maruggi, G.; Shan, H.; Li, J. *Frontiers in Immunology* **2019**, *10*, 594.
- (3) Polack, F. P.; Thomas, S. J.; Kitchin, N.; Absalon, J.; Gurtman, A.; Lockhart, S.; Perez, J. L.; Pérez Marc, G.; Moreira, E. D.; Zerbini, C., et al. *New England Journal of Medicine* **2020**, *383*, 2603–2615.
- (4) Conger, K. Stanford biochemist works with gamers to develop COVID-19 vaccine, <https://scopeblog.stanford.edu/2020/05/20/stanford-biochemist-works-with-gamers-to-develop-covid-19-vaccine/>, 2020.
- (5) Swift, R.; Cha, S.; Morales, N. J. How Pfizer vaccine could be cold comfort for some Asian nations, <https://www.reuters.com/article/us-health-coronavirus-vaccines-pfizer-as/how-pfizer-vaccine-could-be-cold-comfort-for-some-asian-nations-idUSKBN27Q1G1>, 2020.
- (6) Wayment-Steele, H. K.; Choe, C. A.; Nicol, J. J.; Wellington-Oguri, R.; Sparberg, R. A. P.; Huang, P.; Das, R., et al. *BioRxiv* **2020**.
- (7) Van Rossum, G.; Drake, F. L., *Python 3 Reference Manual*; CreateSpace: Scotts Valley, CA, 2009.
- (8) Martin Abadi et al. TensorFlow: Large-Scale Machine Learning on Heterogeneous Systems, Software available from tensorflow.org, 2015.
- (9) Chollet, F. et al. Keras, <https://keras.io>, 2015.
- (10) Pedregosa, F. et al. *Journal of Machine Learning Research* **2011**, *12*, 2825–2830.
- (11) McKinney, W. In *Proceedings of the 9th Python in Science Conference*, ed. by van der Walt, S.; Millman, J., 2010, pp 56–61.
- (12) Harris, C. R. et al. *Nature* **2020**, *585*, 357–362.
- (13) Hunter, J. D. *Computing in Science & Engineering* **2007**, *9*, 90–95.
- (14) Lorenz, R.; Bernhart, S. H.; Zu Siederdissen, C. H.; Tafer, H.; Flamm, C.; Stadler, P. F.; Hofacker, I. L. *Algorithms for molecular biology* **2011**, *6*, 1–14.

- (15) Do, C. B.; Woods, D. A.; Batzoglou, S. *Bioinformatics* **2006**, *22*, e90–e98.
- (16) Eterna OpenVaccine: mRNA Vaccine Degradation Prediction, <https://www.kaggle.com/c/stanford-covid-vaccine/overview>, 2020.
- (17) Wong, S. C.; Gatt, A.; Stamatescu, V.; McDonnell, M. D. In *2016 international conference on digital image computing: techniques and applications (DICTA)*, 2016, pp 1–6.
- (18) Smith, C.; McGuire, B.; Huang, T.; Yang, G. History of Artificial Intelligence, <https://courses.cs.washington.edu/courses/csep590/06au/projects/history-ai.pdf>, 2006.
- (19) Kotsiantis, S. B.; Zaharakis, I. D.; Pintelas, P. E. *Artificial Intelligence Review* **2006**, *26*, 159–190.
- (20) Mitchell, M.; Taylor, C. E. *Annual Review of Ecology and Systematics* **1999**, *30*, 593–616.
- (21) Kaartemo, V.; Helkkula, A. *Journal of Creating Value* **2018**, *4*, 211–228.
- (22) Goodfellow, I.; Bengio, Y.; Courville, A., *Deep Learning*, <http://www.deeplearningbook.org>; MIT Press: 2016.
- (23) Schmidhuber, J. *CoRR* **2014**, *abs/1404.7828*.
- (24) Emmert-Streib, F.; Yang, Z.; Feng, H.; Tripathi, S.; Dehmer, M. *Frontiers in Artificial Intelligence* **2020**, *3*, 4.
- (25) Kim, R. Debate on the Relationship between Neural Network and the Brain. <https://wp.nyu.edu/yungjurick/2020/03/15/debate-on-the-relationship-between-neural-network-and-the-brain/>, 2020.
- (26) Yu, Y.; Si, X.; Hu, C.; Zhang, J. *Neural computation* **2019**, *31*, 1235–1270.
- (27) Hochreiter, S.; Schmidhuber, J. *Neural Comput.* **1997**, *9*, 1735–1780.
- (28) Cho, K.; van Merriënboer, B.; Gülcühre, Ç.; Bougares, F.; Schwenk, H.; Bengio, Y. *CoRR* **2014**.
- (29) Kipf, T. N.; Welling, M. *CoRR* **2016**, *abs/1609.02907*.

5 Appendix

5.1 Figure 12 - Hot encoding

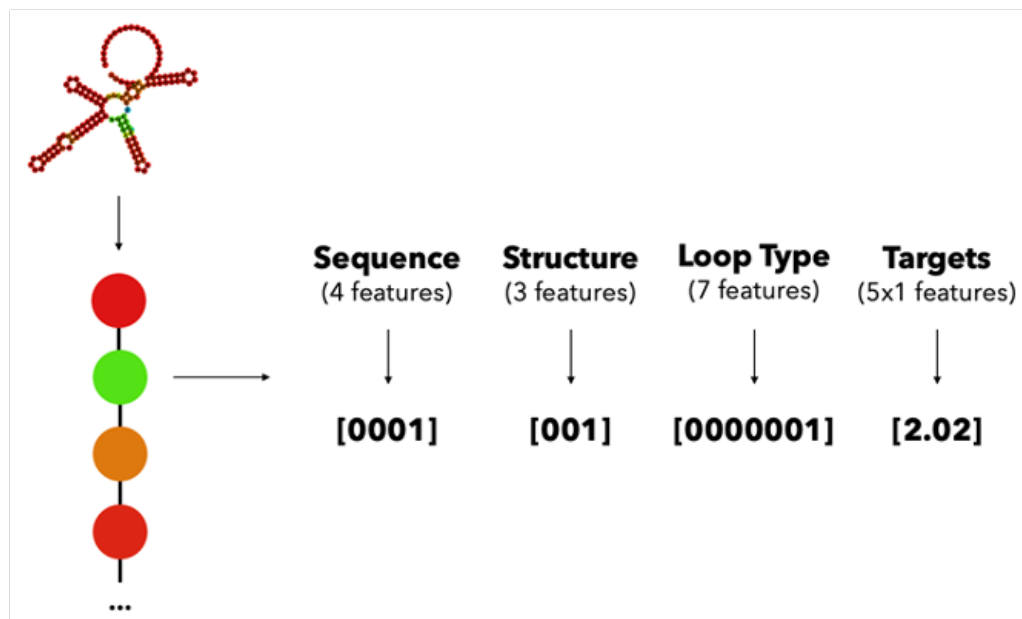


Figure 12: Hot encoding process for the features that are described in Table 2 (produced by author).

5.2 Figure 13 - Basic Artificial Neural Network Architecture

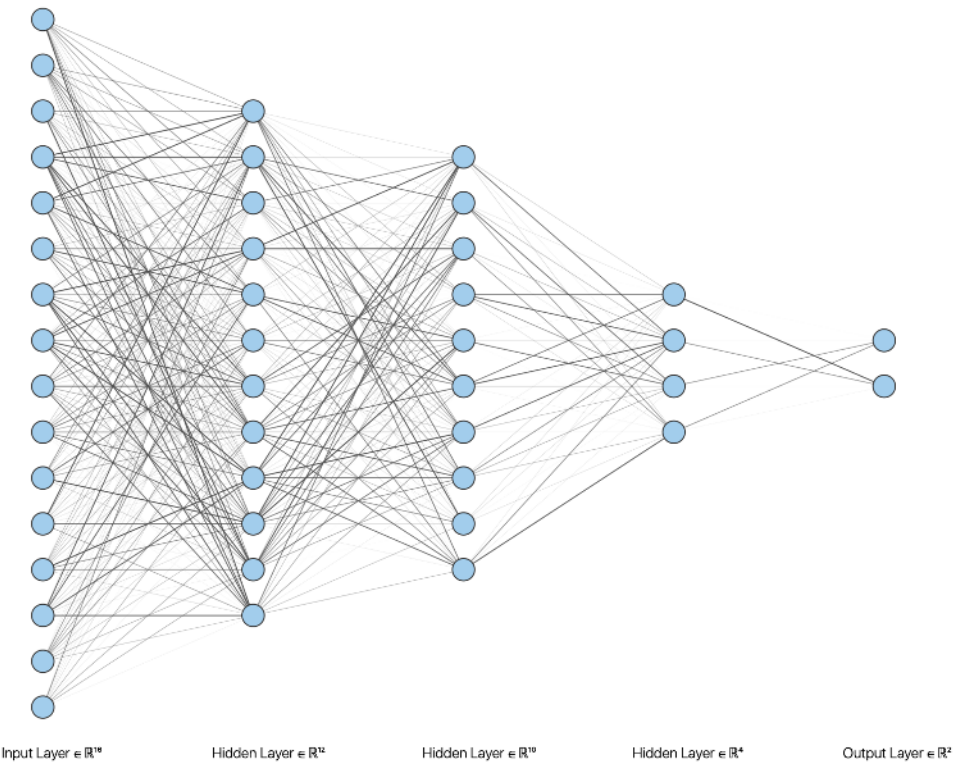


Figure 13: Simple visualization of an Artificial Neural Network with neurons (blue), and four (one input, two hidden, one output) fully connected layers (produced by author).

5.3 Figure 14 - LSTM Diagram

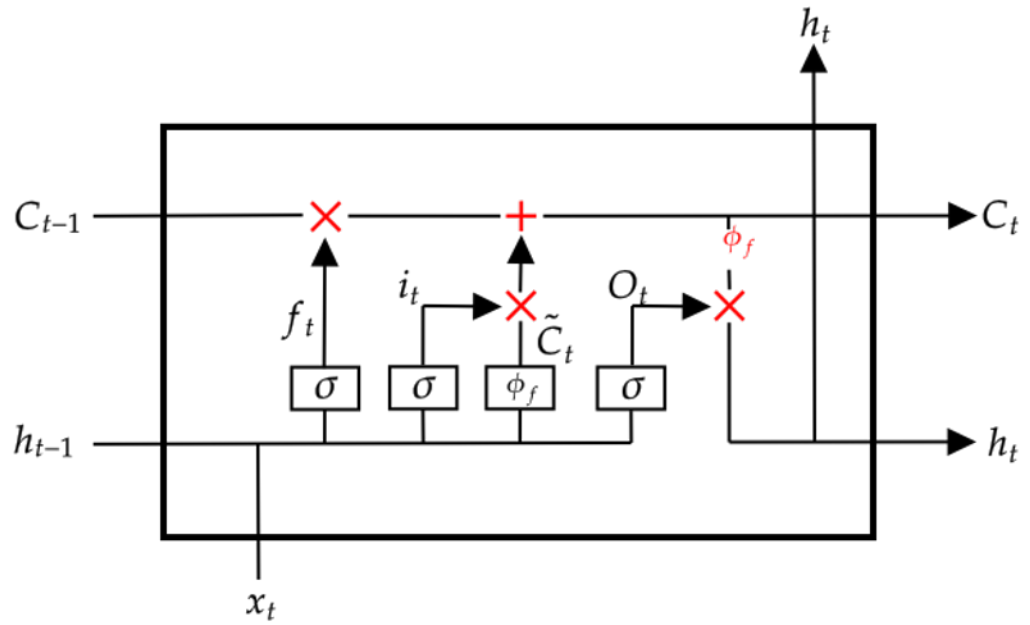


Figure 14: A diagram visualization of equations 2 - 7 i.e. of a single cell in a Long Short Term Memory Network (produced by author).

5.4 Figure 15 - GRU Diagram

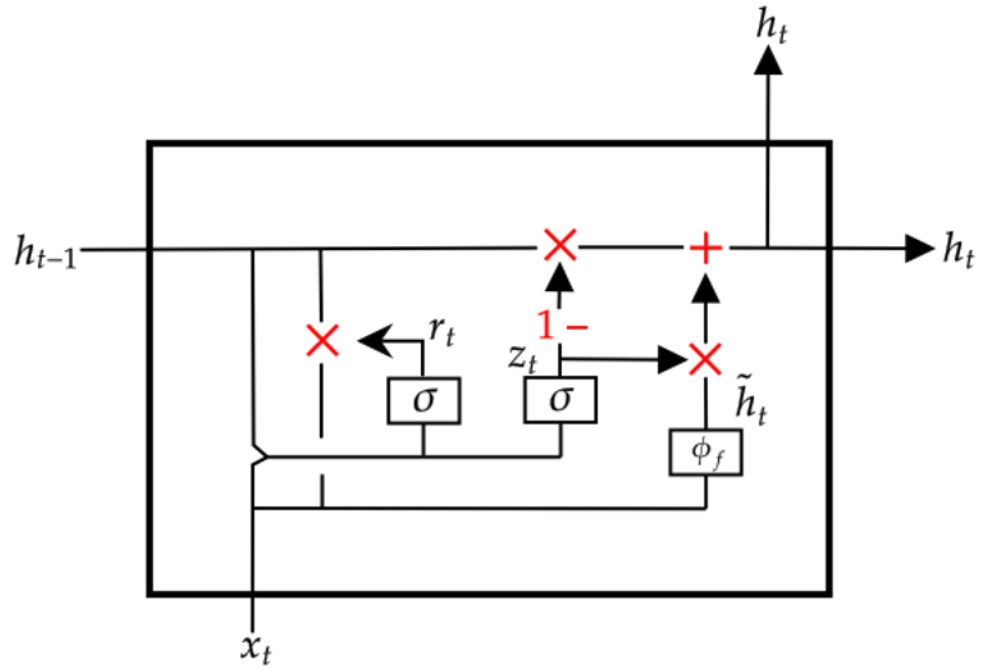


Figure 15: A diagram visualization of equations 8 - 11 i.e. of a single cell in a Gated Recurrent Unit Network (produced by author).

5.5 Figure 16 - GCN Diagram

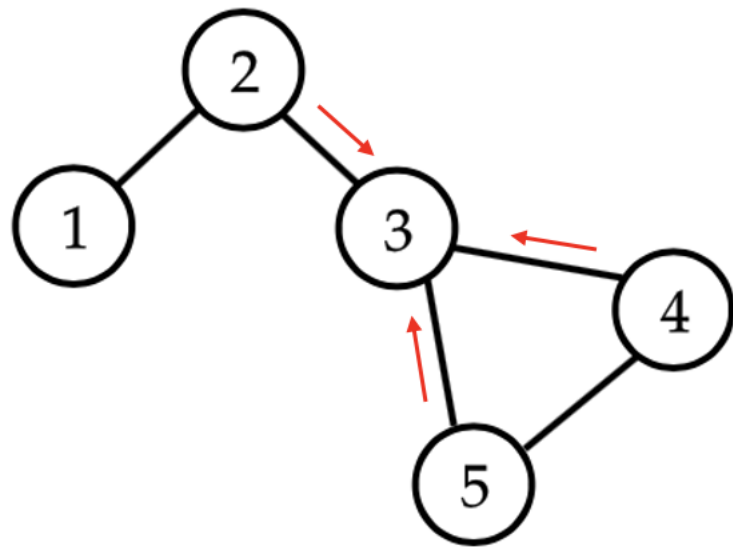


Figure 16: A diagram visualization of an aggregation in a Graph Convolutional Network that then proceeds to follow equation 12 (produced by author).

5.6 Figure 17 - Loss Function Error Term Comparison

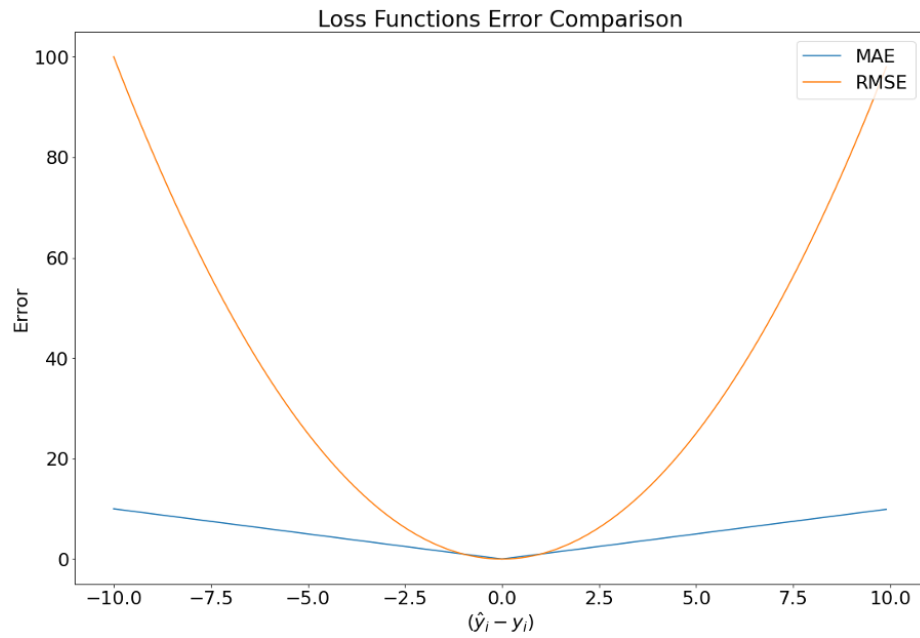


Figure 17: A simple graph to visually illustrate the differences in the error terms between the quadratic one in RMSE and the absolute one in MAE (produced by author).